Author Manuscript

Author Manuscript

Author Manuscript

Author Manuscript

HHS Public Access

Author manuscript

Mater Des. Author manuscript; available in PMC 2022 November 14.

Published in final edited form as:

Mater Des. 2022 November ; 223: . doi:10.1016/j.matdes.2022.111142.

"Fatigue-Crack Propagation Behavior in Microcapsule-Containing Self-Healing Polymeric Networks"

Ana P.P. Fugolin[*],

Jack L. Ferracane,

Carmem S. Pfeifer

Oregon Health & Science University, Restorative Dentistry Department – Division of Biomaterials and Biomechanics, 2730 S Moody Avenue, Portland, OR 97201, United States

Abstract

Over the last years, research on the design of dental self-healing polymers has grown dramatically. It is related to the promising potential of maximizing the clinical lifespan of dental restorations that this strategy holds. In this manuscript, the microcapsule-based strategy is innovated by incorporating the high toughness component N,*N*-Dimethylacrylamide (DMAM) into the healing agent systems and analyzing in-depth the change in crack propagation behavior induced by the addition of microcapsules into the highly crosslinked polymeric network. In general, the addition of the hydrophilic and high vapor pressure DMAM into the healing agent systems imposed a challenge for the microencapsulation, which highlighted the importance of tailoring the properties of the capsules' shells according to the core composition. The addition of DMAM as cushioning agent proved to be a successful strategy since it resulted in increased G'/G" crossover time from 0.06 (control) to 0.57 s and decreased storage modulus from 8.0 (control) to 0.5GPa. In addition, the incorporation of microcapsules within the polymerized networks provided obstacles to crack propagation, which translated to an overall reinforcement of the polymeric network, as evidenced by the increase in toughness up to 50 % and energy required to propagate cracks up to 100 % in systems containing DMAM at 20 wt%.

Graphical Abstract

This is an open access article under the CC BY-NC-ND license (http://creativecommons.org/licenses/by-nc-nd/4.0/).

[*]Corresponding author. fugolin@ohsu.edu (A.P.P. Fugolin).

Declaration of Competing Interest

The authors declare that they have no known competing financial interests or personal relationships that could have appeared to influence the work reported in this paper.

Author Manuscript Author Manuscript Author Manuscript Author Manuscript

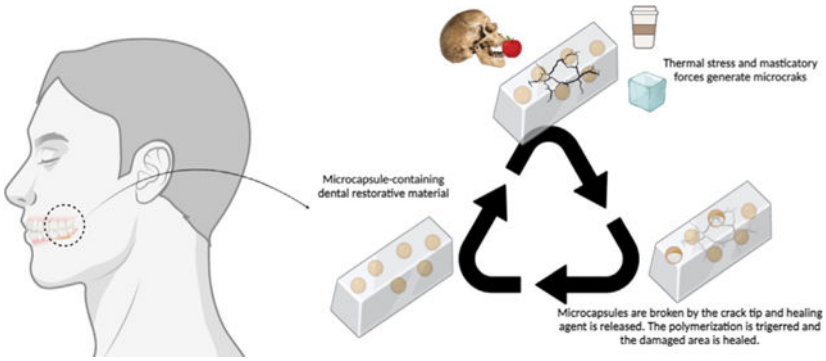

1. Introduction

The development of biomimetic polymeric models capable of autonomic repairing fatigue microcracks has been considered a promising strategy to optimize the functional lifetime of brittle thermosetting networks [1]. The healing of the damaged area restores the mechanical properties and inhibits further propagation as the polymer is subjected to dynamic loading cycles [42]. Among the available approaches to enable thermoset polymers to autonomically repair, the embedding of healing agent-containing microcapsules into the organic matrix has been the most common. In these systems, a low viscosity compound, intended to act as healing agent, is kept sequestered within the capsule, and is released as the microcrack propagation triggers the rupture of the capsule shell [6]. As the healing agent flows to the damaged zone, its polymerization takes place by an amine-peroxide redox reaction, promoting microstructural recovery [6,39,41]. One relevant shortcoming of the microcapsule-based self-healing systems is that their healing capacity is limited by the number of non-reusable, single lifecycle microcapsules incorporated. However, this is the technique with the highest compatibility with the traditional processes employed to manufacture polymers and, therefore, the one with the strongest bench to bedside translational potential.

The advances in self-healing dental polymers have followed the same approach used in other industries, and microcapsule-based systems composed of triethylene glycol dimethacrylate (TEGDMA) sequestered within poly(urea–formaldehyde) shells have been designed and tested. Although the results have shown healing efficiency of 75 % with systems containing microcapsules at 10 wt% [40], critical concerns remain, including the brittleness of the healed area, limitations of the *in vitro* crack induction technique typically employed to validate the systems in which V-notch fracture toughness bars are broken catastrophically and the two halves then placed back into the mold to heal, and a gap in understanding of the impact of the incorporation of microcapsules on the biomechanical behavior of the dental polymeric network. Addressing these concerns is vital to make microcapsule-based self-healing dental materials clinically viable, and a few potential strategies can be proposed.

A promising strategy is to include a high toughness compound as part of the healing system. The tertiary monofunctional acrylamide, N,*N*-Dimethylacrylamide (DMAM), has been used as a high toughness additive in polymeric networks. DMAM-containing hydrogels

Author Manuscript Author Manuscript Author Manuscript Author Manuscript

showed superior mechanical resistance and shape memory ability, which seems to be related to intermolecular H-bonds formed between molecules [38]. In addition, DMAM-containing hybrid polymeric networks have resulted in highly stretchable compounds with the ability to self-heal autonomously at room temperature [3]. These characteristics were attributed to the unique capability of the DMAM compound in acting simultaneously as hydrogen-bonding donor and acceptor, and establishing hydrophobic and supra-intermolecular interactions [3]. The feasibility of the incorporation of DMAM in highly cross-linked dental polymers was also previously investigated and significant refinements in the mechanical properties were noticed [11,14]. Therefore, the replacement of part of the TEGDMA with DMAM seems to be a promising alternative to enhance the mechanical properties of the healed area and to improve the material's capability of absorbing continuous dynamic stress.

In addition to the material-derived challenges, validation of the effectiveness of the healing additions can greatly benefit from alternative techniques to both induce and analyze crack propagation. The most commonly used method to study these systems relies on the production of v-notch fracture toughness bars that are loaded until catastrophic failure, with the healing efficiency calculated by comparing the toughness of the virgin and post-healed bars [39,40]. Although this provides important insight into the overall performance of the system, the mechanism for recovery with these polymers relies on changes at a microstructural level, and this is difficult to elucidate with macroscopic-level tests. In the present investigation, the double torsion fracture toughness technique, which has been used previously for dental composites [15], is proposed as an analytical tool to induce a crack in a standardized fashion and then to study its propagation kinetics through the microcapsule-containing polymer network. This allows for analysis of the energy-dissipation potential by stress relaxation, reflecting the microstructure of the material rather than the macroscopic insight gained from catastrophically failed specimens.

The overall aim of this three-phase study is to encapsulate pre-screened high toughness healing agent systems into poly (urea–formaldehyde) shells and investigate the crack propagation kinetics in dental polymeric networks modified by the addition of these microcapsules. The tested hypotheses are: (1) DMAM-containing healing agents will be properly encapsulated into poly (urea–formaldehyde) shell walls by an oil-in-water double emulsion reaction, (2) the healing agent systems composed of DMAM and TEGDMA will show enhanced toughness, and (3) crack propagation will show an altered and more beneficial profile in microcapsule-enriched dental resin formulations.

2. Materials and methods

2.1. Creating experimental healing agent systems

TEGDMA (triethylene glycol dimethacrylate) was combined with DMAM (N,*N*-dimethylacrylamide) at 0, 20, 40, 60 and 80 wt %, then mixed with either 2 wt% N,*N*-dihydroxyethyl-p-toluidine (DHEPT) or 1 wt% benzoyl peroxide (BPO). These conditions were set in order to reproduce the *in-situ* redox polymerization reaction conditions (1 wt% DHEPT and 0.5 wt% BPO) of the released healing agents when the capsules embedded into the dental polymeric matrix are broken during crack propagation.

Author Manuscript Author Manuscript Author Manuscript Author Manuscript

2.1.1. Polymerization kinetics—For each experimental system, 250 ll of the mixture from each one of the two flasks were mixed in 2 mL clear glass vials placed in the chamber of a Fourier Transform Infra-red spectrometer (Nicolet 6700, ThermoScientific, USA) while near-IR spectra were collected in real-time with 2 scans per spectrum at 4 cm^{-1} resolution for 30 min (n = 3). The degree of conversion (DC) was calculated based on the area of the vinyl peak of the methacrylate (6165 cm^{-1}) and acrylamide (6152 cm^{-1}), and the maximum polymerization rate (RP_{MAX}) as the first derivative of the degree of conversion vs time curve.

2.1.2. Rheological properties—Rheological properties were assessed in a parallel plate rheometer (DH-R, TA Instruments, New Castle, DE, USA). For each tested system, 250 μl of the mixture from each flask were mixed and immediately placed between 20 mm diameter aluminum plates separated by a 300 μm gap (n = 5). Shear storage modulus (G') and G'/G" crossover time (representing gelation point) were assessed in oscillatory mode (1 Hz, 1 % strain) for 30 min.

2.2. Microcapsule synthesis and characterization

For encapsulation, based on the screening tests reported in section 2.1, we selected the compositions with the highest concentrations of DMAM with degree of conversion statistically similar to the control group 100 T. These three systems were composed of 100 wt% TEGDMA (**100 T**), 80 wt% TEGDMA: 20 wt% DMAM (**80 T:20D**), and 50 wt% TEGDMA: 50 wt% DMAM (**50 T:50D**), and were encapsulated in poly(urea–formaldehyde) shells via *in-situ* thermopolymerization (*Note that 50 T:50D was substituted for 40 T:60D because the latter did not result in a two phase reaction and therefore could not be microencapsulated*). The healing agent systems (oil phase) are encapsulated via an oil-in-water double emulsion reaction stabilized by ethylene-maleic anhydride (surfactant), the capsule being formed by a reaction between urea, resorcinol and formaldehyde catalyzed by ammonium chloride (water phase). As negative control, particles of poly (urea–formaldehyde) (**PUF particles**) were also synthesized via in-situ polymerization, following the procedures described above, though these particles were not spherical as they had not been subjected to the double emulsion reaction.

2.2.1. Double emulsion reaction—The oil-in-water double emulsion reactions were performed according to protocols extensively described previously in the literature [8,40]. The amounts of the shell wall and healing agent compounds were decreased by half in order to decrease the overall mass of the synthesized microcapsules without changing the shell-wall forming/healing agent's ratio. In summary, 50 mL of Millipore water was mixed with 13 mL of 2.5 % (wt/vol) EMA (ethylene-maleic anhydride) aqueous solution at room temperature in a 250 mL two-neck round bottom flask. The reaction vial was suspended in a water bath placed on a magnetic hotplate stirrer (IKA C-MAG HS 7 Control Magnetic Hotplate Stirrer). In one of the necks, a temperature sensor (PT1000, IKA) was connected to the hotplate stirrer in order to closely monitor the reaction temperature.

A 50 mm × 20 mm stir bar was placed into the reaction flask, the solution agitated at 300 rpm, and the reaction temperature raised to 55 °C (2 °C/min). After temperature

Author Manuscript Author Manuscript Author Manuscript Author Manuscript

stabilization, 1.25g of urea, 0.125g of ammonium chloride, and 0.125g of resorcinol were added into the mixture and the pH was raised to 3.5 by adding 20 drops of 1 M NaOH. The agitation rate was increased to 400 rpm and 30 mL of healing agent compounds mixed with DHEPT at 1 wt% were added dropwise into the reaction vial. After allowing 10 min for emulsion stabilization, 3.15g of 37 % aqueous solution of formaldehyde was added dropwise into the mixture and the reaction glassware (round bottom flask and water bath) wrapped with aluminum foil. The reaction proceded under continuous agitation for 4 h at 55 °C in order to allow isothermal polymerization of the shell wall membrane. At the end of this period, the agitation and the heating were turned off and the reaction was cooled to room temperature before undergoing gentle vacuum-filtration and air-drying for 24 h in a chemical fume hood. The resultant capsules were stored at 4 °C.

2.2.2. Optical microscopy—The synthesized capsules were examined by an optical microscope (AmScope Stereo Microscope with 5MP Digital Camera) at 10x and 20x magnification immediately after the synthesis and the drying procedures. The diameter of the capsules was measured from the micrographs using ImageJ software (National Institutes of Health, Bethesda, MA). In general, the diameter of 46 (±5) microcapsules were measured for each group.

2.2.3. Extraction in acetone—In order to quantify the encapsulated healing agent, 1 g (w_1) of the synthesized microcapsules was mixed with 10 mL of acetone in a 15 mL Falcon tube and sonicated for 1 min under 50 W, 20 kHz, and 0.7 s and 0.3 s pulse on and off (Benchmark Pulse 150 EU, TE Equipment) (n = 3). The Falcon tubes were centrifuged at 8000 rpm for 10 min, the supernatant (acetone + healing agent) carefully aspirated with a syringe, and the tubes stored in an oven at 37 °C. The weight of the shell walls was measured daily until it stabilized (w_2). The healing agent percentage was calculated according to the following equation:

$$\%HealingAgent = \frac{(w1 - w2)}{w1} \times 100$$

2.2.4. Thermogravimetric analysis (TGA)—For the thermogravimetric analysis, approximately 15 mg of the newly synthesized microcapsules were placed in a platinum pan and subjected to a heat ramp from 30 °C to 850 °C at 10 °C/min (Discovery TGA55, TA Instruments—Waters LLC, New Castle, DE) (n = 3). Percent mass loss was recorded as a function of temperature and average total mass loss calculated for each experimental group. The mass loss vs time curves provided a qualitative assessment of the final composition of the healing agent within the particles.

2.3. Microcapsules-Containing dental resins

Microcapsules were incorporated at 10 wt% in a monomer mixture of BisGMA:BisEMA:UDMA:TEGDMA (wt% ratio: 2:2:2:1, respectively), with 1 wt% BAPO and 0.5 wt% BPO. All the photocuring procedures were performed with a mercury arc lamp (Acticure 4000, EXFO, Mississauga, ON, Canada, filtered to 320–500 nm) at 1000 mW/cm^2

Author Manuscript Author Manuscript Author Manuscript Author Manuscript

reaching out the top surface of the samples. Formulations with no capsules or containing empty PUF particles only were tested as controls.

2.3.1. Polymerization kinetics—Rubber molds (6 mm diameter and 0.8 mm thick) were filled with the experimental dental resins (n = 3), sandwiched between glass slides, and photoactivated for 3 min with the light guide placed 1.5 cm away from the glass surface and delivering 1000 mW/cm^2 at the sample surface. Spectra were collected in real time with 2 scans per spectrum at 4 cm^{-1} resolution. The final degree of conversion was calculated based on the change in area of the carbon–carbon double bond of the methacrylate peak (6165 cm^{-1}), and the maximum polymerization rate (RP_{MAX}) as the first derivative of the degree of conversion vs time curve.

2.3.2. Crack propagation—Crack formation was induced and propagation assessed by the double torsion fracture toughness method, according to ASTM E1820 [15,33]; Testing and Materials 2015). Resin plates (30 mm length × 10 mm width × 2 mm thickness) were produced in split metal molds sandwiched between two glass slides and the resin photoactivated at 1000 mW/cm^2 for 120 s each on the top and bottom surfaces (n = 5). A sharp notch of 5 mm in length was created at the center of one of the 10 mm sides of the sample by inserting a razor blade into the metal mold (Fig. 1A). In order to ensure that the entire surface of the specimen was irradiated and to prevent the need for consecutive and overlapping light exposures, the light guide tip was kept 7 cm away and the power density calibrated to deliver 1000 mW/cm^2 to the surface of the specimen. The extended cure time was employed to ensure homogenous polymerization along the entire specimen.

After 24 h in dry storage, the samples were placed onto the testing jig (Fig. 1B) (Odeme Dental Research, Luzerna, SC, Brazil) assembled on a universal testing machine (MTS Criterion, Eden Prairie, MN, US). To ensure that the specimens were consistently in contact with the spheres on the upper loading actuator, a thin layer of wax was placed between the supporting rods and the lower steel plate, and the samples were loaded with a force of 15 N. The samples were then loaded at a cross-head speed of 0.03 mm/min in order to induce a sharp pre-crack. The loading cycle was immediately stopped when a sudden drop in the load was noticed in the load–displacement graph. The end of each loading cycle is well marked by a descending straight line in the graph, which allowed us to standardize the test. Two subsequent loadings were performed until a crack of approximately 10 mm (±1 mm) in length became evident on the top surface of the specimens (Fig. 1C). Samples that showed irregular crack profiles (e.g., propagation of the crack away from the center of the specimen toward the sides or longer cracks after the 3rd cycle due to slight heterogeneous distribution of the load or microstructural defects) were considered outliers and these specimens were replaced. Cracked samples were stored dry at 37 °C for 48 h to provide time for healing, and then the specimen was again subjected to the same testing sequence. An estimate of the energy required to propagate the crack for each cycle (kN s) was calculated based on the area of the load (kN) vs time (s) curves. For the fracture toughness (K_I - MPa m$^{1/2}$) calculations, first the thickness correction factor (Ψ) was determined using the following equation [5]; Salem et al. 2006):

Author Manuscript Author Manuscript Author Manuscript Author Manuscript

$$\psi = 1 - 1.2604\frac{d}{w} + 2.40\frac{d}{w}exp\left(-\pi\frac{W}{d}\right) \quad (1)$$

where $\boldsymbol{W}$ is the plate width (10.0 mm) and $\boldsymbol{d}$ the specimen thickness (2.0 mm). The Ψ correction factor accounts for the finite size of the torsion arms and was used to calculate the K_I (MPa mm1/2) from [5]; Salem et al. 2006):

$$K_I = P_{max}W_m\left(\frac{3(1+\upsilon)}{Wd^4\psi}\right)^{1/2} \quad (2)$$

where $\boldsymbol{P_{max}}$ is the maximum applied force (N), $\mathbf{W_m}$ the moment arm (0.003 m), and **v** the Poisson's ratio (0.32).

2.4. Statistical analysis

All data being was tested for normality and homoscedasticity (Anderson-Darling and Levene tests, respectively), and then the results were statistically analyzed with one-way ANOVA and Tukey's test for multiple comparisons (α = 0.05).

3. Results

Kinetics of polymerization and rheological properties of the healing agent systems are shown in Figs. 2 and 3, respectively. RP_{MAX} ranged from 2.84 ± 0.16 to 2.12 ± 0.13 % s^{-1} and the addition of DMAM at 40 wt% or above significantly reduced the rates in comparison to the control group (0 % DMAM). Conversely, the DC at RP_{MAX} was significantly reduced in relation to the control only in the system composed of 80 % DMAM (42.3 ± 2.8 vs 50.7 ± 2.7 %, respectively). The numerically highest conversion was registered with incorporation of DMAM at 20 wt% (90.1 ± 1.8 %), and the lowest was recorded at 80 % DMAM 77.4 ± 2.5 %). There was no difference in final DC for 0 and 40 wt% DMAM. Regarding the time to crossover (G'/G"), which is used as a proxy for gelation, the values ranged from 0.04 to 0.58 s with incremental increases of DMAM concentrations above 20 wt%. An opposite trend is seen for shear storage modulus, with the lowest results found for 80 wt% DMAM (0.47 ± 0.03 GPa), and highest (8.25 ± 0.21 GPa) in the formulations containing 20 wt% DMAM.

The quantitative and qualitative characterization results of the newly synthesized microcapsules are presented in Fig. 4. The optical micrographs provide clear evidence for healing agent encapsulation, showing small air bubbles into the core and wrinkles on the surface of the round-shaped capsules with diameters ranging from 5 to 200 μm. The PUF particles presented irregular geometry and size under 50 μm (Fig. 4A and 4B). The percentage of encapsulated healing agent in relation of the overall mass of the capsules ranged from 61.5 ± 4.0 to 41.0 ± 0.7 % for 100 T and 50 T:50D, respectively. As expected, the PUF particles (negative control) showed minimal mass change (2.26 ± 0.2 %). Thermogravimetric curves displaying weight loss (%) as a function of temperature (°C) for the synthesized capsules showed that the increase in DMAM concentration into the

Author Manuscript Author Manuscript Author Manuscript Author Manuscript

formulations leads to a shift of the curves to lower temperatures, i.e., DMAM is lost at lower temperatures so the overall mass loss takes place at higher rates (Fig. 4C).

Results for polymerization kinetics and double torsion fracture toughness are presented in Figs. 5–7 and Table 1. The incorporation of microcapsules did not significantly impact RP_{MAX}, nor DC at RP_{MAX}, which ranged from 15.3 ± 0.2 to 16.4 ± 0.5 % s^{-1} and 38.9 ± 0.9 to 44.1 ± 1.3 %, respectively. The final DC values ranged from 95.8 ± 1.5 and 88.9 ± 2.2 % and were statistically lower for the microcapsule-containing groups (Fig. 5). In general, microcapsule-containing groups absorbed greater energy for crack propagation than the PUF particles for almost all of the loading cycles, with the values ranging between 4.85 ± 0.81 and 13.65 ± 1.45 kN s (Fig. 6A and B). In terms of fracture toughness (K_I), the values ranged between 0.64 ± 0.06 and 1.23 ± 0.13 MPa $m^{1/2}$ (Fig. 7). As expected, there was a significant correlation between the K_I and the area under the force–time curve for each crack (N m; $R^2 = 0.68$) (Fig. 6B and 7A). A significant difference was observed only between cycles #2 and #5 for the PUF group ($p = 0.04$) (Fig. 7A). The K_I averages of cycles #3 and #4 of each group were analyzed by *t*-test ($p < 0.05$) and no significant differences were found (*p* values ranged between 0.067 and 0.98) (Table 1). Finally, the percentage of K_I in relation to cycle #2 (the first crack propagation after pre-cracking) ranged between 72.5 % and 101.5 % (Table 1).

4. Discussion

The development of dental self-healing polymers may represent an important contribution to the clinical lifespan of resin-based dental restorations, which is mainly shortened by disruptions of the structural integrity of the polymeric networks caused by masticatory forces and thermal stress. While different extrinsic and intrinsic strategies may be used to integrate molecular-level functionality to enable damage repair, impart reprocessability, and ultimately extend service lifetimes for crosslinked polymeric networks, the incorporation of microcapsules has been the first approach tried in dentistry. This is mainly related to the fact that this strategy is compatible with the current traditional techniques employed to design and manufacture dental polymers for clinical use. In this study, a high toughness compound was introduced into a microcapsule-based healing agent system and the impact on the polymeric network was investigated.

The high toughness tertiary monofunctional acrylamide, DMAM, was copolymerized with the traditional healing agent, TEGDMA, at different ratios and the formulations were screened using polymerization kinetics and rheological properties. There was a gradual decrease in reactivity as the concentration of DMAM increased in the systems, with significantly lower polymerization rates at concentrations of 40 wt% or higher. This also affected DC at RP_{MAX} and final DC, but significant decreases only were found when DMAM concentration exceeded 60 wt%. The polymerization rate in this particular monomer combination is affected by (for DMAM and TEGDMA, respectively): (1) the number of polymerizable functionalities (mono- vs di-functional): difunctional monomers form crosslinked networks and undergo autoacceleration at lower conversions and generally at faster rates [25]; (2) the type of functionality (acryl vs methacryl): acryl monomers have one order of magnitude higher polymerization rate than methacryl monomers due to the

Author Manuscript Author Manuscript Author Manuscript Author Manuscript

fact that the vinyl group is less sterically hindered in the former [28]; and (3) the amount of resonance stabilization at the vinyl group: for acrylamides, the resonance between the lone pair of electrons on the nitrogen and the carbonyl p orbital leads to a sp^2 hybridization of the nitrogen atom, which results in planarity and stability to rotation around the CAN bond [27], as well as resonance stabilization via the carbonyl and increased resistance to nucleophilic attack [30,35]. In summary, even though DMAM is an acryl monomer, steric and electronic effects lead to reduction in reactivity and conversion when used alone and in the mixture with TEGDMA. In addition, the degradation of BPO generates two primary radicals, which are the second least stable reactive species (only more stable than methyl radicals) [37]. Combined with the slower, diffusion-controlled radical generation in redox systems, this also explains why no conversion was observed in 100 % DMAM. In general, for healing agent purposes, this slower conversion rate is actually advantageous, because the released healing agent needs time to flow through the entire damaged area, completely filling it, and then polymerize, so this may represent an improvement in relation to the purely methacrylate-based healing agent systems which may react too quickly.

The time to G’/G” crossover is used to estimate the onset of gelation and is characterized by a steep increase in viscosity during the polymerization reaction [12]. The incorporation of DMAM into TEGDMA systems at concentrations higher than 20 wt% led to a monotonic increase of the G’/G” crossover time. This directly correlates with the polymerization kinetics profile, the differential reactivity of TEGDMA and DMAM as explained above, and primary cyclization of TEGDMA, which leads to increase in conversion but does not contribute to network formation and gelation [13,32].

Contrary to what was observed for the time to G’/G” crossover, the storage modulus (G’) values showed a monotonic decrease for DMAM concentrations higher than 20 wt%, as expected. G’ quantifies the energy stored in the elastic structure of the resin and relates to the toughness of the polymeric network [19]. The resin is also very tough, as seen in the sequence of pictures in Fig. 8 depicting the deformation of the bend bar with the absence of catastrophic fracture and shape recovery upon load removal. The improvement in toughness and shape recovery stems from DMAM’s capability for establishing hydrogen bonding and ion–dipole interactions [2,34], in addition to the potential formation of interchain bonds by both hydrophobic interactions and hydrogen bonding between the methyl groups, which creates a reentrant phase transition [2]. This property has been used to design and synthesize high elongation DMAM-based networks with self-healing capability [2,10]. It is also possible that the differential in monomer reactivity in this mixture has led to the formation of an interpenetrating network (IPN), which is known to increase toughness in crosslinked polymers [18]. In summary, it is evident that the incorporation of DMAM into polymeric networks significantly enhances the strain energy-absorbing ability and imposes resistance to crack formation and propagation, properties that are highly desirable for self-healing agents [36].

Based on the rheological properties results, it was concluded that it would be beneficial to replace TEGDMA with the highest possible ratios of DMAM in order to obtain systems with optimized toughness. However, the results showed that the threshold ratio of DMAM was 60 wt% to produce maximum DC. Therefore, the systems 40 T:60D and 80 T:20D

Author Manuscript Author Manuscript Author Manuscript Author Manuscript

(to allow a better understanding of the effects of DMAM incorporation) were selected to be encapsulated in PUF shells. However, the formulation 40 T:60D was not sufficiently hydrophobic to result in a two-phase reaction (oil and water), which is a *sine qua non* condition for the formation of microdroplets and, ultimately, microcapsules. Therefore, the DMAM concentration was reduced by 10 wt%, which resulted in successful two-phase reaction formation for the 50 T:50D system. To serve as controls, 100 T and solid PUF particles were synthesized as well. After the 4 h-thermopolymerization reaction was completed, 20 ll of the liquid containing capsules was carefully collected and analyzed by optical microscopy at 10x and 20x magnification. The micrographs showed characteristic spherical morphology with diameters ranging from 5 to 200 μm. The presence of wrinkles on the surface and air voids/bubbles within their core are key features that confirm a successful encapsulation process [6]). The wrinkling of the shells is likely related to two main reasons: (1) the higher vapor pressure of DMAM, which leads to a sequential expansion–contraction of the capsule's core during the concurrent shell formation [22]; and (2) the leakage of healing agent from the core of the microcapsules after the synthesis and/or during the filtration process, leading to an increased surface-to-volume ratio [26].

Since images of the capsules are largely absent from the literature, the synthetic procedure to be followed in this study needed to be significantly optimized from what is presented in other works. First, to confirm the leakage of the healing agent, microcapsules were synthesized using 80 T:20D healing agents containing an aggregation-causing quenching dye with fluorescence at 570 nm to allow for better imaging (Fig. 9A). With this, it was clear that the acetone rinse and vacuum drying procedures recommended in previous publications was leading to the loss of most of the healing agent volume (Fig. 9B). The acetone rinsing was likely plasticizing the shell walls and accelerating the leakage process, which is consistent with recent findings in the literature [31]. Therefore, the protocol was optimized to include purely water-based rinsing, which resulted in significant increase in retention of the healing agent. Of note, microcapsules containing DMAM had much more pronounced loss of healing agent and higher degree of wrinkling of the microcapsule shell in comparison to 100 T (Fig. 9C). This is due to DMAM's high hydrophilicity (LogP = 0.20, compared with LogP = 1.42 for TEGDMA. *LogP, or octanol–water partition coefficient, is a measure of the hydrophilicity or hydrophobicity of a compound*), as well as its low molecular weight and low viscosity, which dramatically increases the driving force for the healing agent transfer across the microcapsule shell into the aqueous phase [26]. In addition, it has been shown that microcapsules containing more viscous cores are more stable to leakage due to higher elasticity, which makes them more prone to absorb the stress on the shell material during the handling of capsules [17,24]. Interestingly, the presence of wrinkles on the microcapsules surface may be beneficial since it provides mechanical interlocking between the microcapsules and the organic matrix and, ultimately, enhanced mechanical properties of the microcapsule-containing dental resins [4,20,26].

Another interesting aspect is that the capsule's yield varied among the different groups. In general, the yield decreased as the DMAM concentration in the healing agents increased. In addition, with the current protocol, the DMAM-containing microcapsules subjected to an extraction assay had significantly lower mass of healing agent in comparison to the 100 T control. It is well known that many parameters affect microencapsulation efficiency and,

Author Manuscript Author Manuscript Author Manuscript Author Manuscript

among them, the core/shell weight ratio seems to play a crucial role (ratios of 6.45/1 and 6.2/1 are the most common used in the PUF microcapsules synthesis) [6,8]. However, when highly hydrophilic compounds, such as DMAM, are added into a double emulsion reaction environment, part of the acrylamide likely migrates from the oil phase to the aqueous phase, which disturbs the core/shell ratio, reducing the amount of microdroplets formed and, ultimately, the encapsulation efficiency. This was likely compounded here by the low molecular weight of DMAM compared with TEGDMA, making diffusion out of the capsule easier, as explained. This was not done here, but this effect may be easily minimized by carefully decreasing the amount of surfactant to increase the interfacial tension between the oil and water phases. Finally, thermogravimetric analysis demonstrated a clear tendency for weight loss (%) at much lower temperatures (°C) as the concentration of DMAM in the capsules increased. This is due to the three-orders of magnitude difference in vapor pressure (DMAM = 7.8×10^{-1} mmHg and TEGDMA = 9.4×10^{-4} mmHg), and twofold difference in boiling point (DMAM = 80–81 °C at 20 mmHg and TEGDMA = 170–172 °C at 5 mmHg), due to DMAM's lower molecular weight and weaker intermolecular forces. It is important to mention that, although these methods do not allow for objective quantification of healing agent encapsulation, there is a clear trend toward the more successful encapsulation of healing agent systems composed of increasing ratios of DMAM.

In the last phase of this study, the impact of the incorporation of microcapsules into dental resin formulations was investigated. The incorporation of microcapsules did not significantly affect the RP_{MAX} or DC at RP_{MAX}, but the final DC showed a 5–7 % reduction with the incorporation of microcapsules, with or without healing agents. Two factors are likely at play here: (1) the increase in viscosity resulting from the incorporation of microcapsules reduced the mobility of the reactive species within the polymerization medium, and (2) the presence of healing agent within the microcapsules added monomers (i.e. vinyl groups) to the matrix, and the lack of conversion of the healing agent within the capsules likely skewed the calculation of the overall conversion of the material. However, this may not result in clinically significant impact since, in general, the systems had high final DC values (ranged from 95.8 % and 88.9 %).

The double torsion fracture toughness technique was tailored to allow standardized induction of cracks as well as the monitoring of their propagation. In general, the presence of microcapsules within the polymeric network led to an increased toughness, which is mainly related to the delayed catastrophic fracture (i.e. more cracks could be propagated for each specimen before failure) since these groups showed similar or higher peak load values than the PUF particles group. It is important to consider that in a crack propagation environment, there is a continuous competition between the intrinsic damage mechanisms occurring ahead of the crack front and the extrinsic mechanisms for crack shielding or increased toughness [9,21]. The simple presence of microcapsules in a polymeric network may improve the response to internal stress by reducing the energy at the crack tip through crack bridging (the crack uses energy by "jumping" around the capsule) [23]. This phenomenon occurs most frequently when the microcapsule size is of the order of the crack-tip plastic zone size [9], which is a region around the crack tip where plastic deformation occurs [7], and the closer the microcapsule size is to the crack-tip plastic zone, the better the crack tip stress is relaxed to a new equilibrium state [23]. It has been

Author Manuscript Author Manuscript Author Manuscript Author Manuscript

shown that if the plastic zone is sufficiently large to encompass most of the capsules in its path, a toughening mechanism similar to those observed for monotonic fracture is triggered [9]. The enhanced toughness is also correlated with a fracture plane morphology change from mirror-like to hackle markings with subsurface microcracking [9], as evidenced by the scanning electron micrographs of representative double torsion resin bars with and without microcapsules (Fig. 10).

In addition to the toughening mechanism, the flow of the unpolymerized healing agent into the crack plane may also play a key role on the increased energy required to propagate the crack. This is likely due to the hydrodynamic pressure imposed by the healing agent, which reduces the effective range of mode-I (or opening) stress intensity [9;17;30]. Therefore, the movement of the viscous liquid into the crack area shields the crack tip, because forces tending to squeeze the healing agent out of the crack during the load removal, and capillary forces tending to draw fluid into the crack, are both occurring during loading [9]; Galvin and Naylor 1964a; [29]. Since the hydrodynamic pressure increases as the healing agent viscosity increases, the higher viscosity of the 100 T system in comparison to the 80 T:20D and 50 T:50D systems may have contributed to the slightly better performance of the 100 T group. The differences in volume of encapsulated healing agent, as suggested by the degrees of wrinkling of the microcapsules, may also have dampened the potential enhancements that could be gained by the incorporation of the high toughness DMAM monomer.

Another interesting finding is related to the fracture toughness results. In general, the values were consistent across the cycles for all the microcapsule-containing groups, which is likely due to the network healing and the mechanical reinforcement of the adjacent area promoted by the presence of the microcapsules, as discussed above. On the other hand, in the PUF particles group, the cycle #5 showed significant lower value than the cycle #2, which is expected since this group is endowed with no healing capability. Cycles #3 and #4 were compared since the #3 is the last one before healing and the #4 is the first one after, which means that cycle #4, at least partially, propagated through a healed zone. This is evidenced by the obvious crack healing observed on fracture toughness specimens, and the fact that that for the PUF particle samples, only 2 post-healing load cycles could be performed prior to catastrophic fracture instead of 3 post-healing cycles for the specimens containing the particles with healing liquid (Fig. 7C). The statistical similarity between cycles #3 and #4 may indicate that the rupture of the microcapsules did not compromise the mechanical properties of the material, which is a concern related to the microcapsule-based self-healing polymers. Although the polymer film formed by the polymerization of the healing agent seems to be capable of filling the area at where the original capsule was entrapped, it was not clear if the presence of a great fraction of broken microcapsules might act as voids or defects and compromise the mechanical strength of the material over time. In addition, it may be reasonable to consider that the KI percentage of the cycle #4 in relation cycle #2 (first cycle after pre-cracking) indicates the healing efficiency of the microcapsule-containing groups. Therefore, our systems showed between 77.0 % and 94.4 % toughness recovery, which may hold great potential as strategy to maximize the clinical lifespan of dental restorations.

Author Manuscript Author Manuscript Author Manuscript Author Manuscript

5. Conclusion

In this study, the incorporation of DMAM monomer into healing agent systems was introduced as an option to improve the performance of microcapsule-based self-healing dental polymers. In addition, cracks were induced and monitored using a more clinically relevant model without breaking the specimens catastrophically and repositioning them to allow healing. The replacement of TEGDMA with DMAM proved to be a promising strategy due to the increase in toughness observed and the capability of undergoing reversible bonds presented by DMAM-containing networks (as shown in recent studies published by other fields). However, there is still much room for improvement in these formulations, for example, by further optimization of the DMAM encapsulation through the double-emulsion technique. Future studies are being designed to tailor the properties of the microcapsule shell walls and to optimize the rinsing/drying processes in order to impose even higher resistance to DMAM efflux during the synthetic procedures. Also, attempting new encapsulation techniques based on methods employed in pharmaceutical industry is an option. Finally, the presence of microcapsules proved to significantly change the response of the polymeric network to mechanical loading, which addresses untapped aspects that may be considered for the development of self-healing resin-based materials.

Acknowledgement

The authors acknowledge the National Institute of Dental and Craniofacial Research for funding **(K99/R00 DE028876)**.

Data availability

Data will be made available on request.

Data Availability

The raw data required to reproduce these findings are available from the corresponding author upon reasonable request.

References

[1]. Aïssa B, Therriault D, Haddad E, Jamroz W, Self-healing materials systems: Overview of major approaches and recent developed technologies, Adv. Mater. Sci. Eng 2012 (2012) 1–17.

[2]. Akhmetzhan A, Myrzakhmetova N, Amangeldi N, Kuanyshova Z, Akimbayeva N, Dosmaganbetova S, Toktarbay Z, Longinos SN, A short review on the n, n-dimethylacrylamide-based hydrogels, Gels. 7 (4) (2021) 234. [PubMed: 34940294]

[3]. Algi MP, Okay O, Highly stretchable self-healing poly (n, n-dimethylacrylamide) hydrogels, Eur. Polym. J 59 (2014) 113–121.

[4]. Alizadegan F, Mirabedini SM, Pazokifard S, Moghadam SG, Farnood R, Improving self-healing performance of polyurethane coatings using pu microcapsules containing bulky-ipdi-ba and nano-clay, Prog. Org. Coat 123 (2018) 350–361.

[5]. Becker T, Marrow T, Tait R, An evaluation of the double torsion technique, Exp. Mech 51 (9) (2011) 1511–1526.

[6]. Blaiszik B, Caruso M, McIlroy D, Moore J, White S, Sottos N, Microcapsules filled with reactive solutions for self-healing materials, Polymer 50 (4) (2009) 990–997.

Author Manuscript Author Manuscript Author Manuscript Author Manuscript

[7]. Broek D, The crack tip plastic zone. Elementary engineering fracture mechanics, in: Broek D (Ed.), Elementary Engineering Fracture Mechanics, Springer Netherlands, Dordrecht, 1986, pp. 91–114.

[8]. Brown EN, Kessler MR, Sottos NR, White SR, In situ poly (urea-formaldehyde) microencapsulation of dicyclopentadiene, J. Microencapsul 20 (6) (2003) 719–730. [PubMed: 14594661]

[9]. Brown EN, White SR, Sottos NR, Fatigue crack propagation in microcapsule-toughened epoxy, J. Mater. Sci 41 (19) (2006) 6266–6273.

[10]. Cheng Y.u., Ren K, Huang C, Wei J, Self-healing graphene oxide-based nanocomposite hydrogels serve as near-infrared light-driven valves, Sens. Actuators, B 298 (2019) 126908.

[11]. Consani RLX, Paula AB, Fugolin APP, Pfeifer CS, Strategies for potential toughening of acrylic denture bases polymerized with microwave energy, Brazilian dental journal. 31 (2020) 523–531. [PubMed: 33146337]

[12]. Dörr D, Kuhn U, Altstädt V, Rheological study of gelation and crosslinking in chemical modified polyamide 12 using a multiwave technique, Polymers. 12 (4) (2020) 855.

[13]. Elliott JE, Lovell L, Bowman C, Primary cyclization in the polymerization of bis-gma and tegdma: A modeling approach to understanding the cure of dental resins, Dent. Mater 17 (3) (2001) 221–229. [PubMed: 11257295]

[14]. Fugolin AP, Dobson A, Mbiya W, Navarro O, Ferracane JL, Pfeifer CS, Use of (meth) acrylamides as alternative monomers in dental adhesive systems, Dent. Mater 35 (5) (2019) 686–696. [PubMed: 30826074]

[15]. Fujishima A, Ferracane JL, Comparison of four modes of fracture toughness testing for dental composites, Dent Mater. 12 (1) (1996) 38–43. [PubMed: 8598249]

[16]. Galvin GD, Naylor H, Effect of lubricants on the fatigue of steel and other metals, Proc. Inst. Mech. Eng 179 (1) (1964) 857–875.

[17]. Gan SN, Shahabudin N. 2019. Applications of microcapsules in self-healing polymeric materials. Microencapsulation-Processes, Technologies and Industrial Applications.

[18]. Gao G, Wang X, Chen M, Bowman CN, Stansbury JW, Functional nanogels as a route to interpenetrating polymer networks with improved mechanical properties, Macromolecules 54 (23) (2021) 10657–10666.

[19]. Gradin P, Howgate PG, Seldén R, Brown RA, 16 - dynamic-mechanical properties, in: Allen G, Bevington JC (Eds.), Comprehensive Polymer Science and Supplements, Pergamon, Amsterdam, 1989, pp. 533–569.

[20]. Haghayegh M, Mirabedini S, Yeganeh H, Microcapsules containing multi-functional reactive isocyanate-terminated polyurethane prepolymer as a healing agent. Part 1: Synthesis and optimization of reaction conditions, J. Mater. Sci 51 (6) (2016) 3056–3068.

[21]. Hosdez J, Langlois M, Witz J, Limodin N, Najjar D, Charkaluk E, Osmond P, Forre A, Szmytka F, Plastic zone evolution during fatigue crack growth: Digital image correlation coupled with finite elements method, Int. J. Solids Struct 171 (2019) 92–102.

[22]. Ina M, Zhushma AP, Lebedeva NV, Vatankhah-Varnoosfaderani M, Olson SD, Sheiko SS, The design of wrinkled microcapsules for enhancement of release rate, J. Colloid Interface Sci 478 (2016) 296–302. [PubMed: 27309950]

[23]. Kubo A, Umeno Y, Velocity mode transition of dynamic crack propagation in hyperviscoelastic materials: A continuum model study, Sci. Rep 7 (1) (2017) 1–8. [PubMed: 28127051]

[24]. Nesterova T, Dam-Johansen K, Kiil S, Synthesis of durable microcapsules for self-healing anticorrosive coatings: A comparison of selected methods, Prog. Org. Coat 70 (4) (2011) 342–352.

[25]. Odian G 2004. Principles of polymerization. John Wiley & Sons.

[26]. Parsaee S, Mirabedini SM, Farnood R, Alizadegan F, Development of self-healing coatings based on urea-formaldehyde/polyurethane microcapsules containing epoxy resin, J. Appl. Polym. Sci 137 (41) (2020) 49663.

[27]. Pauling L, The nature of the chemical bond. Ii. The one-electron bond and the three-electron bond, J. Am. Chem. Soc 53 (9) (1931) 3225–3237.

Author Manuscript Author Manuscript Author Manuscript Author Manuscript

[28]. Pirman T, Ocepek M, Likozar B, Radical polymerization of acrylates, methacrylates, and styrene: Biobased approaches, mechanism, kinetics, secondary reactions, and modeling, Ind. Eng. Chem. Res 60 (26) (2021) 9347–9367.

[29]. Plumbridge W, Ross P, Parry J, Fatigue crack growth in liquids under pressure, Mater. Sci. Eng 68 (2) (1985) 219–232.

[30]. Robin M, Bovey FA, Basch H. 1970. The chemistry of amides. by Zabicky J, Wiley-Interscience, London. 1–72.

[31]. Shinde VV, Taylor G, Celestine A-D-N, Beckingham BS, Fused filament fabrication 3d printing of self-healing high-impact polystyrene thermoplastic polymer composites utilizing eco-friendly solvent-filled microcapsules, ACS Appl. Polym. Mater 4 (5) (2022) 3324–3332.

[32]. Tanaka Y, Stanford JL, Stepto R, Interpretation of gel points of an epoxy–amine system including ring formation and unequal reactivity: Reaction scheme and gel-point prediction, Macromolecules 45 (17) (2012) 7186–7196.

[33]. Testing ASf, Materials. 2015. Astm e1820: Standard test method for measurement of fracture toughness. ASTM International West Conshohocken.

[34]. Toktabayeva A, Rakhmetullayeva R, Abutalip M, Mamutova A, Batyrbayeva A, Mun G, The new hybrid copolymers based on n-isopropylacrylamide, J. Chem. Technol. Metall 54 (2019) 475–482.

[35]. Toriumi Y, Kasuya A, Itai A, Crystallographic studies on retinoidal-active and-inactive aromatic anilides, J. Org. Chem 55 (1) (1990) 259–263.

[36]. Vasiliev VV, Morozov EV, Chapter 3 - mechanics of a unidirectional ply, in: Vasiliev VV, Morozov EV (Eds.), Advanced Mechanics of Composite Materials, second edition., Elsevier Science Ltd, Oxford, 2007, pp. 57–132.

[37]. Vicentin BLS, Netto AM, Blümich B, Di Mauro E, Identification of free radicals generated by different curing modes in a dental resin cement, Appl. Magn. Reson 47 (9) (2016) 1003–1014.

[38]. Wang F, Yong X, Deng J, Wu Y, Poly (n, n-dimethylacrylamide-octadecyl acrylate)-clay hydrogels with high mechanical properties and shape memory ability, RSC Adv. 8 (30) (2018) 16773–16780. [PubMed: 35540536]

[39]. Wu J, Weir MD, Melo MAS, Xu HH, Development of novel self-healing and antibacterial dental composite containing calcium phosphate nanoparticles, J. Dent 43 (3) (2015) 317–326. [PubMed: 25625674]

[40]. Wu J, Weir MD, Zhang Q, Zhou C, Melo MAS, Xu HH, Novel self-healing dental resin with microcapsules of polymerizable triethylene glycol dimethacrylate and n, n-dihydroxyethyl-p-toluidine, Dent. Mater 32 (2) (2016) 294–304. [PubMed: 26743969]

[41]. Wu J, Xie X, Zhou H, Tay FR, Weir MD, Melo MAS, Oates TW, Zhang N, Zhang Q, Xu HHK, Development of a new class of self-healing and therapeutic dental resins, Polym. Degrad. Stab 163 (2019) 87–99.

[42]. Zhang F, Ju P, Pan M, Zhang D, Huang Y, Li G, Li X, Self-healing mechanisms in smart protective coatings: A review, Corros. Sci 144 (2018) 74–88.

Author Manuscript Author Manuscript Author Manuscript Author Manuscript

HIGHLIGHTS

- A high-toughness healing agent system containing N,*N*-Dimethylacrylamide (DMAM) was specifically designed for microcapsule-based self-healing dental polymers.
- DMAM works as a cushioning agent.
- Microcapsules increase the overall fracture toughness of the material.
- Significant higher energy is required to crack propagation in microcapsule-containing polymers.

Author Manuscript Author Manuscript Author Manuscript Author Manuscript

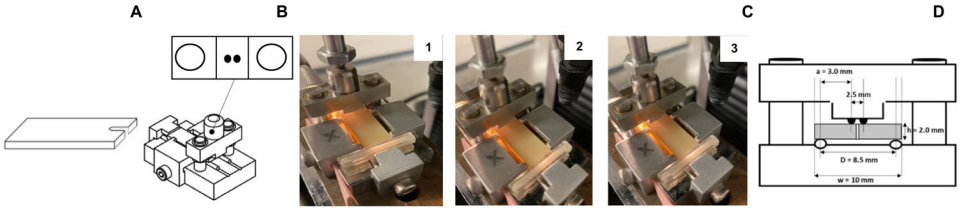

Fig. 1.

(A) Geometry of the specimens designed to assess crack propagation kinetics, **(B)** as well as the 4-point bending jig used to hold and load the specimens (Odeme Dental Research) in the double torsion fracture toughness technique. **(C)** In general, the specimens were loaded 3 times until noticing a crack of approximately 10 mm in length on the surface (white arrows indicate the monitored crack; 1 = first crack from the notch, 2 = second cycle from the crack generated in cycle #1, 3 = third cycle from the crack generated in cycle #2). After cycle 3, the load was completely removed and the specimens were placed in an oven at 37 °C for 48 h. **(D)** Schematic representation of the test geometry and the dimensions of the variables used to calculate fracture toughness. Specimen is represented in grey.

Author Manuscript Author Manuscript Author Manuscript Author Manuscript

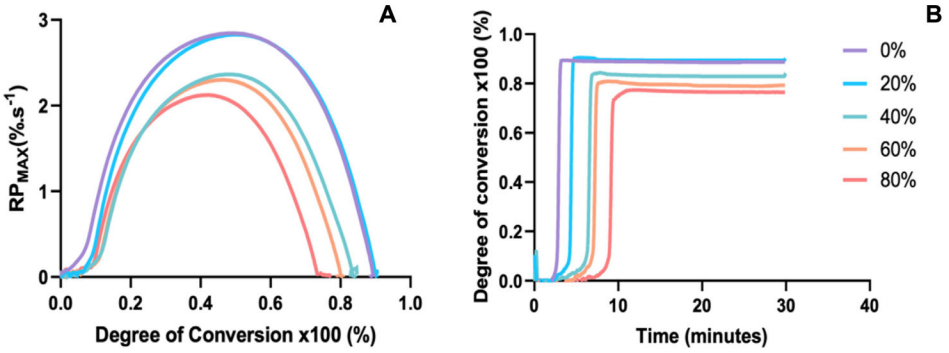

C

Groups	RP_{MAX} (%.s^{-1})	DC at RP_{MAX} (%)	Final DC (%)
0% DMAM	2.84 (0.16) **a**	50.7 (2.7) **a**	89.2 (2.3) **a**
20% DMAM	2.83 (0.22) **a**	50.8 (1.3) **a**	90.1 (1.8) **a**
40% DMAM	2.36 (0.19) **b**	49.2 (1.7) **a**	85.7 (2.9) **ab**
60% DMAM	2.30 (0.12) **b**	46.3 (2.3) **ab**	81.3 (3.1) **b**
80% DMAM	2.12 (0.13) **b**	42.3 (2.8) **b**	77.4 (2.5) **c**
p value	*0.0010*	*0.0041*	*0.0005*

Fig. 2.

(A) Maximum rate of polymerization (RP_{MAX}, %.s^{-1}) as a function of the degree of conversion (x100, %) and **(B)** degree of conversion (x100, %) as a function of the time (minutes) curves for all the experimental healing agent systems with DMAM replacing TEGDMA at 0, 20, 40, 60, and 80 wt%. Note that a formulation composed of 100 % DMAM did not polymerize. **(C)** Average (standard deviation) of RP_{MAX}, degree of conversion at RP_{MAX}, and final degree of conversion for all tested formulations. Different letters indicate significant differences between the groups with different concentrations of DMAM ($p < 0.05$).

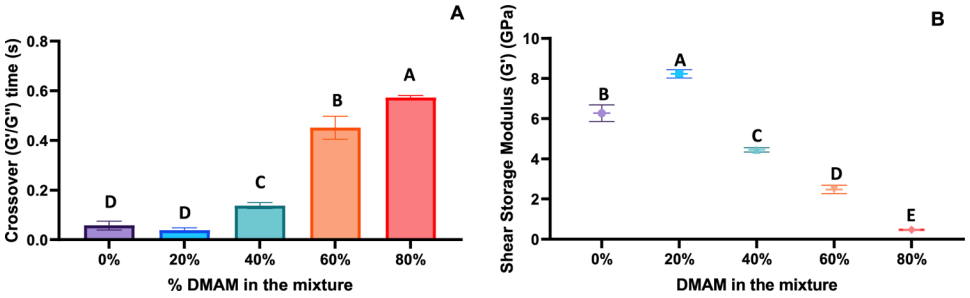

Fig. 3.

(A) Crossover (G'/G") time (in seconds) and **(B)** shear storage modulus (G') (in GPa) for all tested TEGDMA healing agent formulations containing incremental concentrations of DMAM assessed in rheology experiments conducted in shear mode in real time during the polymerization reaction. Different letters indicate significant differences between the groups with different concentrations of DMAM ($p < 0.05$).

Author Manuscript
Author Manuscript
Author Manuscript
Author Manuscript

Author Manuscript Author Manuscript Author Manuscript Author Manuscript

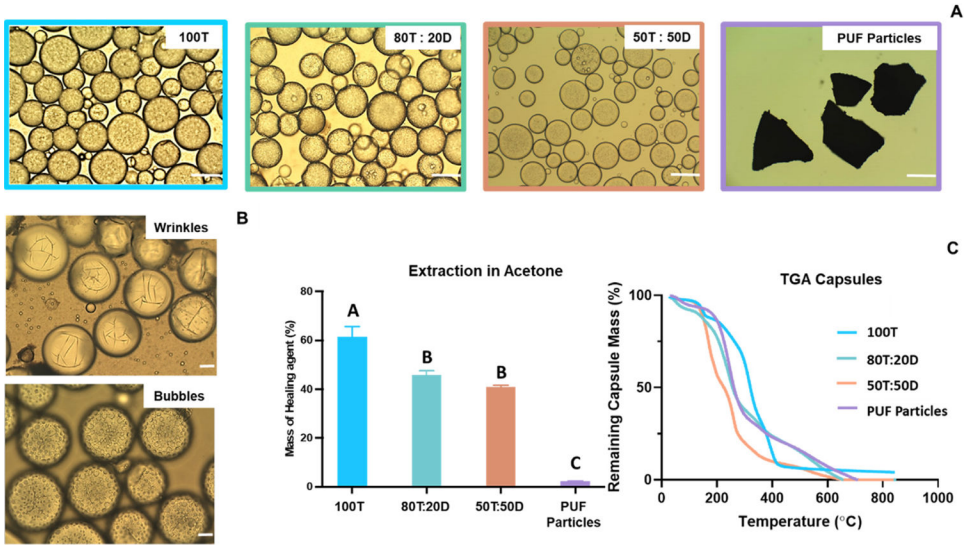

Fig. 4.

(A) Optical micrographs at 20x magnification of the synthesized microcapsules containing 100 wt% TEGDMA, 80 wt% TEGDMA + 20 wt% DMAM, and 50 wt% TEGDMA + 50 wt% DMAM, and the solid poly(urea–formaldehyde) microparticles. White bar on the images corresponds to 10 μm. **(B)** Representative optical micrographs depicting the wrinkles on the shell walls and air voids and bubbles into the core of the synthesized particles, which are considered key indicatives of proper microencapsulation. **(C)** Percentage of encapsulated healing agent in relation to the overall mass of the microcapsules obtained by extraction in acetone for the freshly synthesized microcapsules and solid PUF microparticles. Different letters indicate significant differences between the groups ($p < 0.05$). Weight loss (%) as a function of temperature (°C) for the synthesized microcapsules obtained from thermogravimetric analysis.

Author Manuscript Author Manuscript Author Manuscript Author Manuscript

A

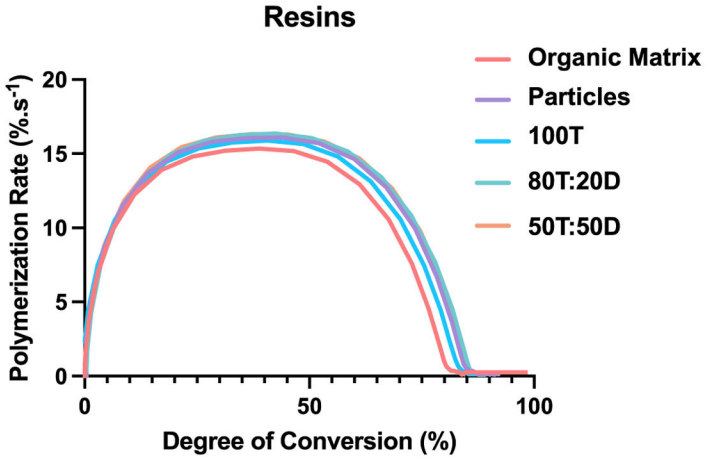

B

Groups	RP_{MAX} (%.s^{-1})	DC at RP_{MAX} (%)	Final DC (%)
Organic Matrix	15.3 (0.2) **a**	38.9 (0.9) **b**	95.8 (1.5) **a**
Particles	16.1 (0.6) **a**	44.1 (1.3) **a**	91.1 (1.3) **b**
100T	15.9 (0.5) **a**	40.8 (2.1) **ab**	89.8 (1.0) **b**
80T:20D	16.4 (0.5) **a**	42.5 (1.9) **ab**	88.9 (2.2) **b**
50T:50D	16.3 (0.5) **a**	39.8 (0.1) **b**	91.1 (1.3) **b**
p value	*0.0994*	*0.0138*	*0.0006*

Fig. 5.

(A) Rate of polymerization (%.s^{-1}) as a function of degree of conversion (%) curves for all experimental dental resins containing microcapsules. Organic matrix and resin containing PUF microparticles were tested as controls. The data was obtained in real time as the samples were photoactivated for 3 min at 1000 mW/cm^2. **(B)** In the table, averages (standard deviation) for maximum rate of polymerization (RP_{MAX}, %.s^{-1}), degree of conversion at RP_{MAX} (DC at RP_{MAX}, %), and final degree of conversion (Final DC, %) are displayed. Values followed by different letters indicate statistically significant differences between the tested formulations ($p < 0.05$).

Author Manuscript Author Manuscript Author Manuscript Author Manuscript

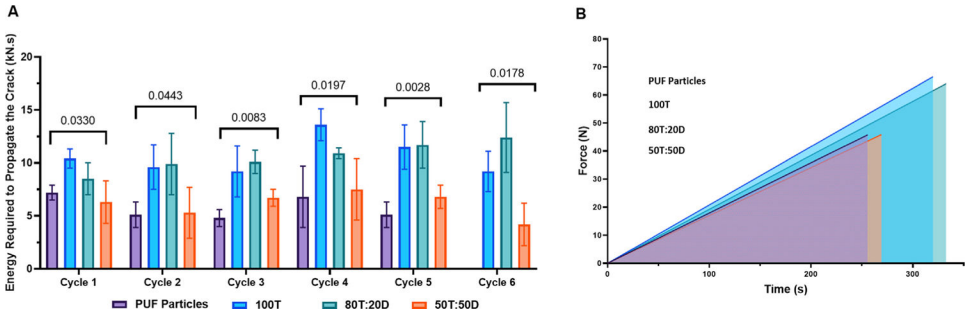

Fig. 6.

(A) Averages and standard deviations of the energy required to propagate the crack (kN·s) for each loading cycle applied on the virgin double torsion bar (cycles 1, 2 and 3) and after healing for 48 h at 37 °C (cycles 4, 5 and 6) for all the tested resin systems containing microcapsules or PUF solid microparticles. The results were obtained from double torsion fracture toughness technique and calculated based on the area of the load (kN) vs time (s) curves. Different letters indicate statistically significant difference among the experimental groups within the same loading cycle ($p \leq 0.05$). **(B)** Diagram force (N) vs time (s) representing the overall energy required to crack propagation in the different experimental groups.

Author Manuscript Author Manuscript Author Manuscript Author Manuscript

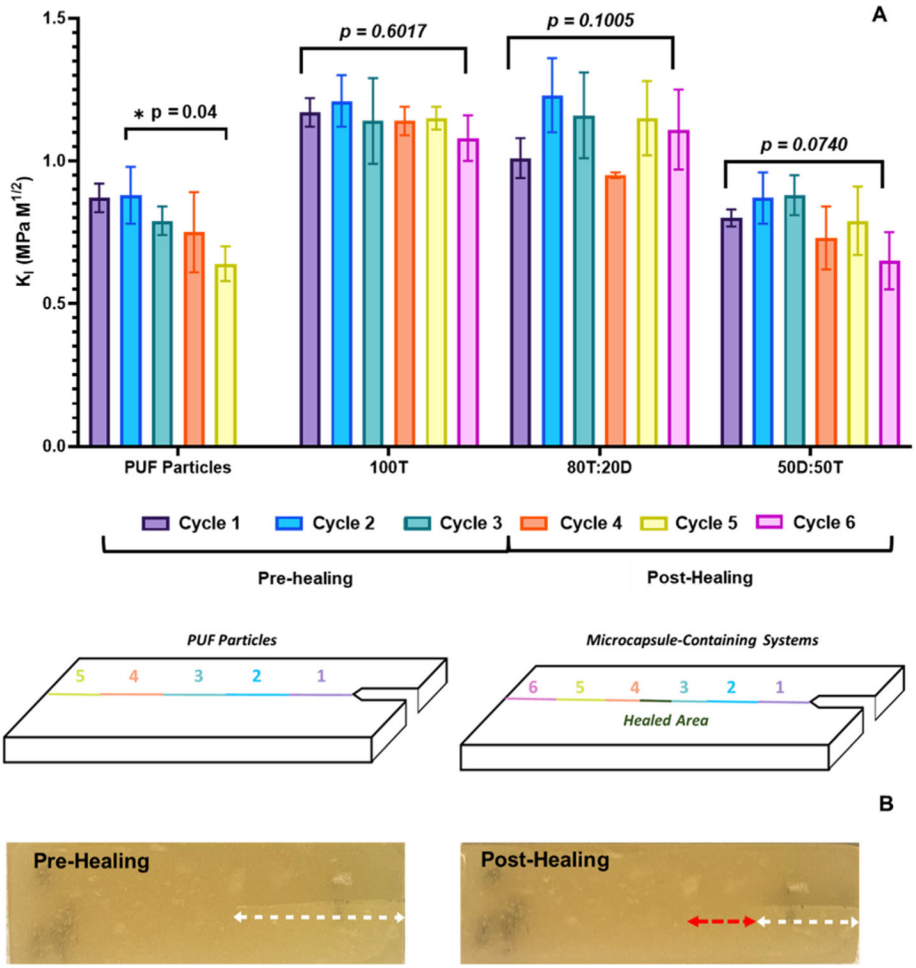

Fig. 7.

(A) Averages and standard deviation of fracture toughness (KI, MPa $m^{1/2}$) for each loading cycle applied on the virgin double torsion bar (cycles #1, #2 and #3) and after healing for 48 h at 37 °C (cycles #4, #5 and #6) for all the tested resin systems containing microcapsules or PUF solid microparticles. Significant differences were found only between cycles #2 and #5 for the PUF Particles (p = 0.04). Below the graph, a cartoon representing the differences in terms of crack propagation profiles for the PUF particles and microcapsule-containing groups. **(B)** Photos of a representative 100 T double torsion specimen immediately after crack induction by the double torsion technique and after healing for 48 h at 37 °C. The length of the induced crack (white arrows) was reduced dramatically after the healing process (red arrow).

Author Manuscript Author Manuscript Author Manuscript Author Manuscript

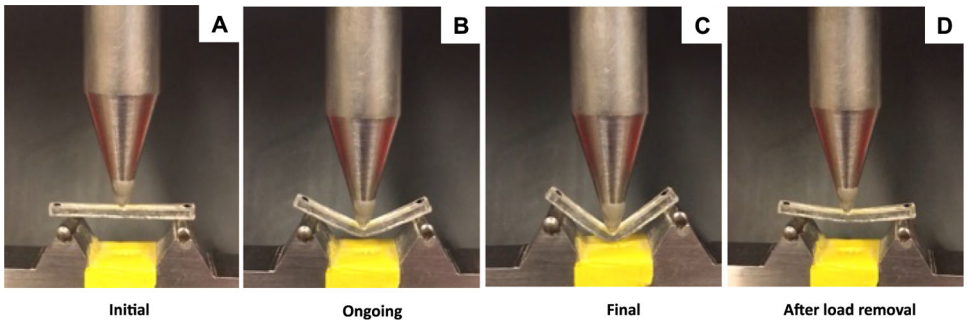

Fig. 8.

Rectangular flexural strength bars (2 mm width, 2 mm thickness, and 25 mm length) loaded in three-point bending. The bars were produced in silicone molds sandwiched between glass slides. The bars are composed of 100 % DMAM and made photopolymerizable by the addition of 0.2 wt% DMPA (2,2-dimethoxy-2-phenylacetophenone) and 0.4 wt% DPI-PF6 (diphenyliodonium hexafluorophosphate). Photoactivation procedures were carried out by a mercury arc lamp filtered to 320–500 nm at 630 mW/cm^2 with exposures for 120 s from the bottom and top surfaces (Exfo Acticure 4000 Mercury Arc Lamp). The tip of the light guide was placed 7 cm away from the top surface of the sample in order to create a spot size large enough to expose the entire bar. After a 24 h dry storage period, the samples were subjected to the three-point bending test, according to ISO 4049. The sample was monotonically loaded (1.0 mm/min) and the beam bent with the angle increasing as the test progressed until the bottom surface of the sample contacted the metal bottom surface of the jig. At this stage, the test was manually stopped and the load removed from the surface of the sample, which recovered its original shape within 5 min.

Author Manuscript Author Manuscript Author Manuscript Author Manuscript

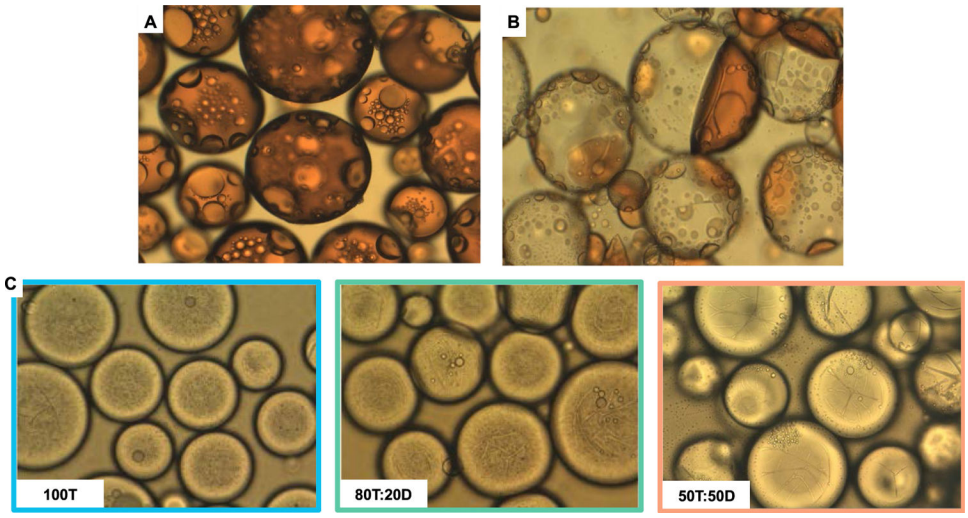

Fig. 9.

Optical micrographs at 20x magnification of DCM-tagged 80 T:20D healing agent encapsulated in poly(urea–formaldehyde) shells before **(A)** and after acetone rinsing and vacuum drying procedures **(B)**. Note the dramatic reduction of healing agent present within the core of the microcapsules. **(C)** Representative optical micrographs at 20x magnification of the newly-synthesized microcapsules showing higher degree of wrinkling on their surface as the concentration of encapsulated DMAM increases.

Author Manuscript Author Manuscript Author Manuscript Author Manuscript

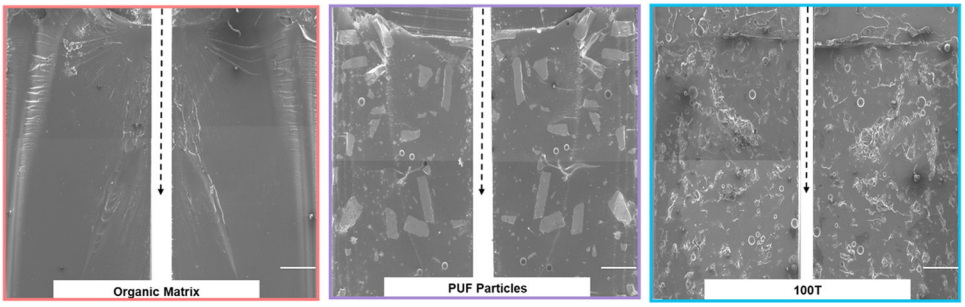

Fig. 10.

Scanning electron micrographs of representative fractured double torsion resin bars with no capsules (organic matrix), with PUF solid particles, and microcapsules containing 100 % TEGDMA. Micrographs were taken at 65x magnification and 15 kV. White bars on the images corresponds to 500 μm and dotted arrows indicate overall crack propagation direction. Of note is a dramatic difference in the fractured area topography among the groups. In the organic matrix group, a clear mirror region following the fracture initiation site is identified, similar to what is seen in a low toughness, brittle glass. Adjacent to the mirror area, a mist region followed by a hackle is shown. For the PUF particles group, these fractography elements are visible but less pronounced than on the unfilled bars. The surface shows that the PUF particles have fractured and the surface is smooth, rather than the crack being deflected around these particles. Finally, the group containing embedded microcapsules shows a different fractured surface with increased hackle markings, a generally rougher surface with evidence of microcapsule exposure or pull-out, and fracture on multiple planes.

Author Manuscript Author Manuscript Author Manuscript Author Manuscript

Table 1

T-test comparisons between the K_I values of cycle #3 (last one before healing) and cycle #4, that likely propagated through the same healed zone, and K_I percentage of the cycles in relation to cycle #2, which was the first one after pre-cracking. Values highlighted in bold correspond to the estimated healing percentage.

T-test comparison between Kj of loading cycles #3 and #4				
Cycles 3 × 4	**PUF Particles**	**100 T**	**80 T:20D**	**50 T:50D**
p value	0.96	0.973	0.067	0.98
K_i percentage of each cycle in relation to loading cycle #2				
Cycles #	**PUF Particles**	**100T**	**80T:20D**	**50T:50D**
1	99.1	96.5	82.0	92.2
2	100.0	100.0	100.0	100.0
3	89.8	94.4	94.0	101.5
4	**84.6**	**94.4**	**77.0**	**83.6**
5	72.5	95.5	92.1	90.6
6	-	89.8	90.3	75.4